

Rapid #: -21785271

CROSS REF ID: 1280439

LENDER: COF (Colorado State University) :: Morgan Library

BORROWER: PUL (Princeton University) :: Interlibrary Services, Firestone

TYPE: Article CC:CCG

JOURNAL TITLE: Reliability engineering & systems safety

USER JOURNAL TITLE: Reliability engineering & system safety.

ARTICLE TITLE: Bayesian updating of solar panel fragility curves and implications of higher panel strength for

solar generation resilience

ARTICLE AUTHOR:

VOLUME: 229

ISSUE:

MONTH:

YEAR: 2023

PAGES: 108896-

ISSN: 0951-8320

OCLC #: 663412430

Processed by RapidX: 12/20/2023 8:30:51 AM

This material may be protected by copyright law (Title 17 U.S. Code)

FISEVIER

Contents lists available at ScienceDirect

Reliability Engineering and System Safety

journal homepage: www.elsevier.com/locate/ress



Check for updates

Bayesian updating of solar panel fragility curves and implications of higher panel strength for solar generation resilience

Luis Ceferino a,b,c,*, Ning Lin c,d, Dazhi Xi d

- ^a Department of Civil and Urban Engineering, New York University, USA
- ^b Center for Urban Science and Progress, New York University, USA
- ^c The Andlinger Center for Energy and the Environment, Princeton University, USA
- ^d Department of Civil and Environmental Engineering, Princeton University, USA

ARTICLE INFO

Keywords: Solar panels Fragility functions Hurricane hazards Bayesian update Structural reliability

ABSTRACT

Solar generation can become a major and global source of clean energy by 2050. Nevertheless, few studies have assessed its resilience to extreme events, and none have used empirical data to characterize the fragility of solar panels. This paper develops fragility functions for rooftop and ground-mounted solar panels calibrated with solar panel structural performance data in the Caribbean for Hurricanes Irma and Maria in 2017 and Hurricane Dorian in 2019. After estimating the hurricane wind fields, we follow a Bayesian approach to estimate fragility functions for rooftop and ground-mounted panels based on the observations supplemented with existing numerical studies on solar panel vulnerability. Next, we apply the developed fragility functions to assess failure rates due to hurricane hazards in Miami-Dade, Florida, highlighting that the panels perform below the code requirements, especially rooftop panels. We also illustrate that strength increases can improve the panels' structural performance effectively. However, strength increases by a factor of two still cannot meet the reliability stated in the code.

1. Introduction

The power system infrastructure is rapidly changing as the world transitions towards cleaner energy sources. Market and government projections state that solar generation will be 20-30% of the global electricity by 2050 [1-4]. In 2019 in the United States, installations of solar generators already accounted for 40% of the electric generating capacity installed [5]. As a result, the resilience of the power system infrastructure is also changing. First, the design standards or the level of exposure of solar energy generating infrastructure can differ from those of current generation infrastructure. For example, engineers design nuclear plants or dams with risk category IV for safety in nuclear and hydroelectric generation, source of 20 and 7% of electricity generation in the United States [6]. This category provides the highest structural reliability levels in the ASCE7-16 design code since failure "could pose a substantial hazard to the community" [7]. In contrast, engineers can design solar panels following conventional reliability levels for rooftops, i.e., risk category II. Engineers can design them with even lower levels, i. e., risk category I, if the solar installation structural failure "represents low risk to human life in the event of failure" as for large ground-mounted installations in remote locations [8]. Moreover, by design, the solar generators themselves must be placed outdoors and are directly exposed to extreme loads such as high winds. This exposure level is markedly different from existing generating units typically within protective infrastructure. For example, natural gas, the source of 40% of the electricity in the United States [6], is often transported in pipes underground and is processed in power plants with key equipment within buildings. As solar generation becomes a key source of our energy production, we need a better understanding of its resilience to natural hazards and ability to provide sufficient and reliable power during extreme load conditions.

Fragility functions describe the likelihood of damage (or failure) due to an extreme load, e.g., earthquake shaking, hurricane wind. The development of fragility functions for energy generation components is essential to understand the risk profile of power systems [9–12]. However, lack of data has prevented the assessment of panel vulnerability to extreme loads, hindering our ability to understand the resilience of future power grids. Due to the lack of solar panel failure data or appropriate experimental tests, Goodman [13] used simplified numerical structural assessment to propose the first solar panel fragility

^{*} Corresponding author at: 370 Jay St, Room 1309, Brooklyn, NY 11201. *E-mail address:* ceferino@nyu.edu (L. Ceferino).

functions. The analysis focused on the yielding onset of rooftop panel racks due to high wind loads. Due to the lack of better models, its fragility function has also been applied to ground-mounted solar panels [10,14].

To the authors' knowledge, data-driven assessments of solar panel vulnerability have not been conducted. In this paper, we fill this research gap by compiling and analyzing a novel dataset of solar panel structural performance in 60 sites in the Caribbean during the 2017 and 2019 hurricane seasons. This dataset captures these storms' severe impact on renewable infrastructure, especially in Puerto Rico [15], including a wider variety of panels' structural failure mechanisms that were represented in the numerical simulation by Goodman [13]. We used our empirical dataset to enhance Goodman [13]'s results and preset the first data-driven fragility functions for both rooftop and ground-mounted solar panels.

Combining multiple information sources, e.g., numerical simulations with ground-truth data of infrastructure damage, can improve fragility function estimations since disaster data is generally scarce. However, rigorously combining different data sources for fragility functions is challenging. At the end of the '90 s, a study first proposed using Bayesian statistics to combine various data sources of earthquake damage and improve fragility functions for concrete buildings [16]. The study was followed by other formulations and implementation of Bayesian statistics to combine multiple data sources for fragility and hazard analyses [17–30].

This paper formulates and implements Bayesian methods to combine different information sources and find more robust estimates of fragility function parameters than those based on either observation or numerical simulation. We present an algorithm based on Metropolis-Hastings (MH) Monte Carlo Markov Chain (MCMC) to solve the Bayesian formulation with computational efficiency. Through the Bayesian approach, we explicitly characterize the uncertainty in the fragility functions' parameters, which is critical to account for the uncertainty in key risk metrics, e.g., panels' annual rate of failure.

Next, this paper shows an application of the developed fragility functions by assessing the structural reliability of solar panels in Miami-Dade, Florida, to hurricanes. Our assessment combines our new fragility functions and hurricane hazard modeling for mainland United States [31]. Finally, this paper explores the value of increasing solar panel

strength in, for example, reducing annual failure rates and meeting different ASCE7-16 standards for structural reliability. This paper contributes to the body of literature on the risk of modern power systems under extreme events by providing the first data-informed fragility functions for solar panels and a holistic assessment of their reliability to hurricanes.

2. Solar panel structural performance data

2.1. Panel damage data

Our dataset is an extended version of the "Solar Under Storm" reports' panel failure dataset [32,33]. The initial dataset consists of 26 sites primarily located in residential buildings in Puerto Rico for rooftop panels. "Solar Under Storm" focuses on reporting main failure mechanisms in rooftop installations with qualitative descriptions of failure modes in the Caribbean after the large hurricanes Irma and Maria in 2017 and Dorian in 2019. The study reports frequent failures in racks and the clips that attach the panel to the racks [32]. Unlike Goodman [13], which covers the early serviceability damage state, i.e., yielding onset in racks, the identified damage conditions in the dataset introduce a damage state of structural collapse (Fig. 1).

Because the "Solar under Storm" dataset focuses on failed rooftop panels, we extended the dataset to cover panels that survived the hurricanes. The data extension is critical to properly fit fragility functions with data representing various panels' structural performance. By surveying local engineers in Puerto Rico, we extended the dataset to 46 sites. Table 1 lists the data attributes, and Supplementary Table 1 shows

Table 1

Data attributes of solar panels' structural performance in the Caribbean after the 2017 and 2019 hurricane seasons. An initial dataset with 26 rooftop installations [32,33] was extended in this study to include other 20 rooftop and 14 large ground-mounted installations.

Rooftop panels	Ground-mounted panels	
Coordinates	Coordinates	
Panel Type (e.g., rail-based metal)	Installation Size (in Mw)	
Failure Type (e.g., clip failure)	Damage extent (in%)	



(a) Residential rooftop panels



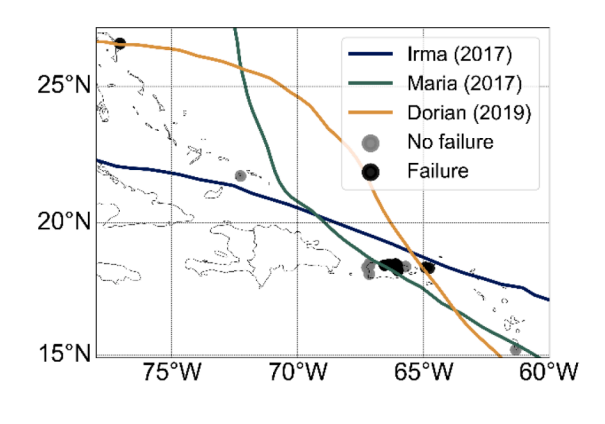
(b) Large ground-mounted panels

Fig. 1. Example of solar panel damage in dataset. (a) Rooftop panels: Clip failures in the bolt connection between panels and racks (red arrows) lead to panel uplift (see bolt in circle at the left with zoom-in view). Clamp failures (see clamp in circle in the middle with zoom-in view) lead to blown racks (see red line where a rack used to be placed) [32]. (b) Large ground-mounted panels: Satellite imagery shows the scale of the wind damage in comparison to the pre-hurricane view in the rectangle [34]. In large-scale failures, multiple failure modes were found, including debris impact from damaged panel arrays.

the full dataset of the rooftop solar panels. Out of the 46 sites, 46% experienced clip (clamp) failures (e.g., Fig. 1a), 17% racking failures, 4% roof attachment failures, and 50% rack or connection, roof attachment failure. Most panels underwent damage due to debris impact (65% in the initial dataset). It is important to note that debris failure was primarily part of a cascading mechanism with projectiles originating from the damaged panels themselves. Fig. 2a shows a map with all the rooftop panel installation sites, indicating clip, racking, or attachment failures. The plot also shows that Hurricane Irma, Maria, and Dorian's tracks were near the sites.

For ground-mounted solar panels, we surveyed reports and newspapers to determine panels' failures in large sites. Utility-scale solar installations are primarily ground-mounted, each one composed of hundreds or thousands of panels. Thus, their failures often have media coverage. We visually verified the installation damage with highresolution satellite imagery from the National Oceanic and Atmospheric Administration (NOAA) [34] and Google Earth Satellite Imagery. We obtained information for 14 large panel installations with 13 MW of capacity on average in the Caribbean for Hurricanes Irma and Maria in 2017. The "Solar Under Storm" study also surveyed a few of these installations, but it did not report the installations' geographical coordinates to preserve the confidentiality of the sites [33]. Table 1 lists the data attributes, and Supplementary Table 2 shows the full dataset these ground-mounted solar panels. 36% of the sites reported significant failures in more than 50% of their panels, including the Humacao Solar Farm (Fig. 1b) with 40 MW of capacity, the second largest solar farm in Puerto Rico [35]. Fig. 2b shows installations indicating the sites with significant failures, i.e., more than 50% of failed panels. The reported failures included clip (clamp) failures, racking fractures and buckling, bolt shear failure, and bolt loosening [33]. We observed evidence of cascading structural failures triggered by debris from damaged panels in large sites, suggesting that damage in a few panels can progress quickly to massive failures. This observation is consistent with the cascading failures of clip (T-clamps) fractures found in the more detailed post-hurricane structural inspections [33].

In Puerto Rico, where 50 and 59% of the inspected rooftop and ground-mounted panels were located, wind design levels range from 63 to 72 m/s and from 57 to 76 m/s for structures with risk categories I and II, respectively [7]. As mentioned earlier, the ASCE7-16 requires solar panels on residential buildings to be designed with a risk category of II. Ground-mounted solar panels can be designed with a risk category I. While the structural design levels for ground-mounted solar panels are lower, our described findings reported fewer sites with large failures than rooftop panels (50% versus 60%). For further assessment, we analyzed the wind conditions that the panels experienced.



(a) Residential rooftop panels

2.2. Wind conditions

We obtained the hurricanes' tracks, their radii of maximum wind, and maximum winds from the revised HURDAT2 Atlantic hurricane database [36]. We estimated axisymmetric winds circulating counter-clockwise based on a tropical cyclone wind profile model [37]. We then combined these circulating winds with the estimated background winds [38] to calculate the resulting asymmetric wind fields for each hurricane. For smoothness, we interpolated HURDAT2 3 h timesteps to obtain maximum wind at each panel site for every 10 min (Supplementary Fig. 1).

For evaluation, we compared the resulting wind estimates to the hourly wind records from the NOAA National Centers for Environmental Information [39]' Global Integrated Surface Dataset during Hurricane Maria from the weather station at the San Juan International Airport in Puerto Rico (Fig. 3). No other stations reported wind data from Puerto Rico for the event. Unfortunately, wind data were not gathered for the most intense period; nevertheless, data during and before August 20th, 2017, show that our wind estimates and records closely follow each other. During August 20th, both datasets showed rapid wind intensification, at least up to ~30 m/s, when records stopped. Our estimates indicate that winds peaked at 60 m/s on August 20th, 2017.

Using a multiplicative factor from an empirical formula [40], we converted the 1-m sustained wind estimates at the panel sites to 3 s gusts to be compatible with the wind load metrics for structural design [7]. Failures in rooftop panels were caused by gusts starting at 73 m/s, with a mean in all sites of 81 m/s (Fig. 4a). Failures in ground-mounted panels

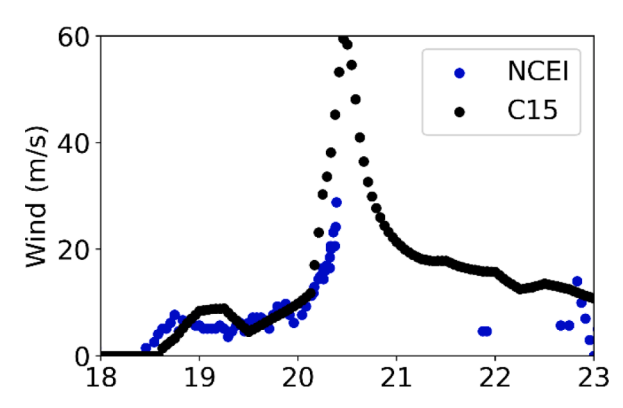
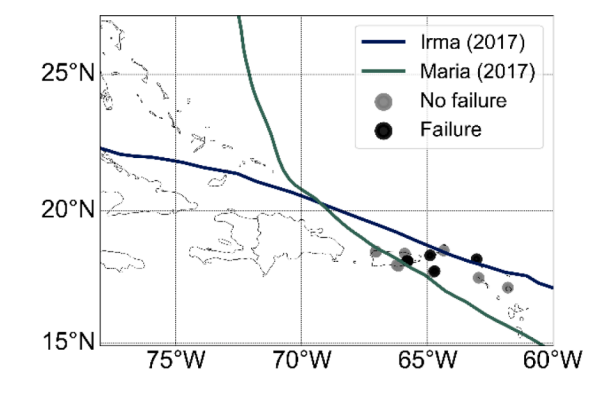
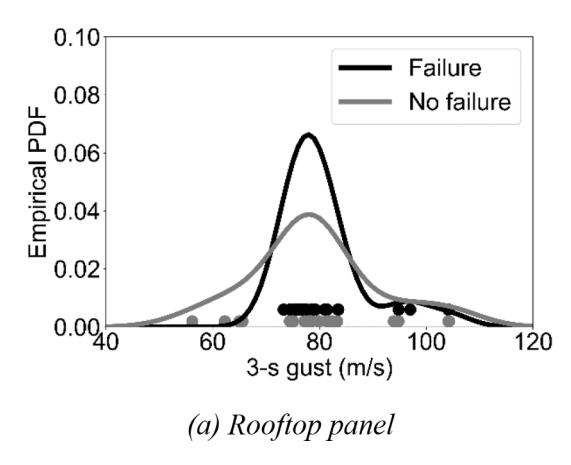


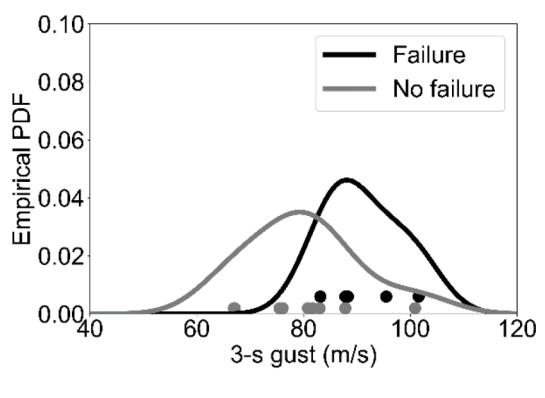
Fig. 3. Comparison of wind estimates and the wind records from NOAA National Centers for Environmental Information [39] at the San Juan International Airport.



(b) Large ground-mounted panels

Fig. 2. Solar panel sites in collected dataset after Hurricanes Irma and Maria in 2017 and Hurricane Dorian in 2019. The lines indicate the hurricane tracks, and the panels with failures (clip, racking, rooftop attachment) and without failures are highlighted in the map. Failure in the panel array is defined as either clip, racking, or roof attachment (in case of rooftop panels) failures in more than 50% of the panels.





(b) Ground-mounted panel

Fig. 4. 3 s gust distributions for panels with (black) and without (gray) damage. The data are shown as points and the empirical probability density functions are estimated using a Gaussian kernel.

were caused by gusts starting at 83 m/s, with a mean of 91 m/s (Fig. 4b). The solar panel dataset is suitable for assessing fragility functions as it contains ranges of gusts where failure occurrence has large variability (Fig. 4). For example, between 70 and 90 m/s, several sites with rooftop panels experienced both failure and no failure. Getting data in this range is critical for fragility functions to appropriately capture the uncertainties in panel failure when transitioning from low winds to high winds.

3. Bayesian framework for fragility function updates

3.1. Fragility function

Fragility functions with lognormal shape are typically used to model infrastructure's damage due to wind hazards and other extreme loads [41–43]. Its shape is given by

$$q(w; v, \beta) = \Phi\left(\frac{\ln(w) - \ln(v)}{\beta}\right) \tag{1}$$

where q is the probability of panel failure due to a wind gust w, v is the wind gust with a failure probability of 50%, β is a normalizing factor, and Φ is the cumulative standard normal distribution function. β defines the width of the transition range between winds with low and high failure probability, and it is a measure of aleatory uncertainty in the vulnerability analysis. In the limit, when $\beta \rightarrow 0$, Eq. (1) becomes equivalent to a deterministic assessment, where the panel would fail after a fixed wind threshold.

We follow a Bayesian approach to fit solar panels' fragility functions due to two key factors.

- The Bayesian formulation can represent fragility functions' significant epistemic uncertainties through random fragility function parameters, v and β . Treating v and β as random variables rather than deterministic parameters allows for the propagation of their uncertainty to solar panel damage predictions in risk analysis.
- The Bayesian approach allows for the combination of multiple sources of information to improve the fragility function characterization. The dataset presented in this paper provides the opportunity for a data-driven, probabilistic description of panel failure. However, the number of samples is not high, e.g., 46 and 14 for rooftop and ground-mounted panels, respectively. Thus, through the Bayesian approach, we use Goodman [13]'s numerical assessment as prior information and then combine it with the dataset for the final fragility function estimates.

In the Bayesian formulation, the posterior distribution $p(v, \beta|x)$ after

combining both data sources is

$$p(v,\beta|x) = \frac{p(x|v,\beta)p(v,\beta)}{\int \int p(x|v,\beta)p(v,\beta)dvd\beta}$$
 (2)

where $x=\{x_1,x_2,...,x_n\}$ is the vector containing the failure information at each site, thus $x_n \in \{0,1\}$ equals zero if the panel did not fail and one if it failed, and n is the number of sites, i.e., equal to 46 and 14 for rooftop and ground-mounted panels, respectively. The limit state for rooftop panel failure is defined as extensive damage, including clip, racking, or roof attachment failures. Hereafter, we refer to this damage state as panel failure. The limit state for failure in the large ground-mounted panels is defined as extensive damage, including clip and racking failures, in more than 50% of their panels. $p(x|v,\beta)$ is the likelihood function of observing the dataset for fixed values of v and ρ , and $\rho(v,\beta)$ is the prior distribution of v and ρ .

3.2. Prior

As in the Bayesian approach, v and β from Eq. (2) are random variables rather than deterministic values. Additionally, v and β can only be positive numbers. We select lognormal distributions to model the prior. Other distributions could also be used, e.g., Gamma distributions, but their implementation falls outside this study's scope. The probability density functions (pdfs) of p(v) and $p(\beta)$ are given by

$$p(v) = \frac{1}{v\sigma_v \sqrt{2\pi}} \exp\left(-\frac{(\ln v - \mu_v)^2}{2\sigma_v^2}\right)$$
 (3)

$$p(\beta) = \frac{1}{\beta \sigma_{\beta} \sqrt{2\pi}} \exp\left(-\frac{\left(\ln \beta - \mu_{\beta}\right)^{2}}{2\sigma_{\beta}^{2}}\right)$$
(4)

where μ_v and σ_v are hyperparameters defining the logarithmic mean and standard deviation of v. μ_β and σ_β are hyperparameters defining the logarithmic mean and standard deviation of β . For simplicity, we assume v and β are independent. Thus

$$p(v,\beta) = p(v)p(\beta) \tag{5}$$

For Bayesian assessments, the data supporting the prior distribution need to be independent of the data used for the parameter update. Thus, the selection of Goodman [13]'s fragility function is appropriate for this study. The numerical assessment is based on code-conforming rooftop panels designed for wind conditions in Atlanta, Georgia. The uncertainty in the fragility function stems maily from the stochastic velocity pressure induced by winds acting on the panel. It also models stochasticity in material strength and construction quality. Goodman [13]'s study is frequentist; thus, the parameters defining the fragility function in Eq. (1)

are deterministic. The resulting fragility functions had a deterministic v, gust for 50%-failure probability, of 60 m/s and β of 0.13 for a panel on a 30° roof.

To use these numerical evaluations as a prior distribution, we adjusted their wind design conditions to the Caribbean. Taking San Juan, Puerto Rico, as a reference, we scaled up v to represent a local solar panel design using the ratio between the wind design values in San Juan and Atlanta. We consider a design with risk category II (wind with a return period of 700 years) for rooftop panels and a risk category I (wind with a return period of 300 years) for the ground-mounted panels [8]. We use resulting values of 85 m/s and 81 m/s as the prior's medians of v for the rooftop and ground-mounted solar panels, respectively, and then estimate the logarithmic means (μ_v) since the median equals the exponential of the logarithmic mean (e^{μ_v}) for lognormal distributions. Similarly, we estimate the logarithmic means of β (μ_{β}) using Goodman [13]'s value of 0.13 as the prior's median for both panel types.

The prior's logarithmic standard deviations (σ_v and σ_θ) are a measure of uncertainty in Goodman [13]'s estimates of v and β . Small values of σ_v and σ_{β} imply that we are certain that Goodman [13]'s study accurately and thoroughly modeled solar panel's structural properties and their behavior under extreme loads. However, capturing actual structural and material properties is difficult as they vary widely according to construction, manufacturing, and installation processes [44,45-47,48]. Additionally, Goodman [13]'s numerical assessment only included failures triggered by bending loads on the racks, without considering the other failure modes observed in the ground-truth data, like clip or roof attachment failures. To account for potentially different structural properties and failure modes, we use σ_v and σ_{β} values equal to 0.5. For the lognormal prior, these values are equivalent to a coefficient of variation of 0.53, a considerable high value representing that actual structural behavior can differ from the numerical simulation. For example, the $\mu \pm 1.5\sigma$ interval for the prior of v is 19 to 173 m/s. We consider this is a reasonable range since failures below 19 m/s are only common for quite vulnerable infrastructure, like old wooden poles from distribution lines [49,50]. Winds above 173 m/s are catastrophic and damage most infrastructure [41,51,52].

3.3. Likelihood of observing the data

Panel failure follows a Bernoulli distribution with probability q that is a function of the wind. Considering that the failures at different n sites are independent, then the likelihood of observing failures or non-failures in n sites is given by

$$p(x|v,\beta) = \prod_{i=1}^{n} q^{x_i} (1-q)^{1-x_i}$$
(6)

where x_i is one if the panel failed at the site or zero otherwise and q is found from the fragility function in Eq. (1) with parameters v and β .

3.4. Posterior distribution

According to the Bayes rule for conditional probabilities, the posterior $p(v,\beta|x)$ can be found in Eq. (2). The numerator is the product of the likelihood of observing the panel failures and the prior distribution. The denominator is the integral of this product through the entire parameter space of v and β . Eqs. (5) and (6) allow us to find the numerator in closed form, but the denominator requires a complex integration that cannot be solved analytically.

3.5. Solving for the posterior distribution using MCMC

To overcome the challenge stemming from numerical integration, we followed an approach based on MCMC [53]. MCMC only requires evaluating a proportional function to the posterior distribution rather than the posterior itself. Thus, we can find samples from the posterior

and circumvent the evaluation of the integral with MCMC since

$$p(v,\beta|x) \propto p(x|v,\beta)p(v,\beta) \tag{7}$$

We use the Metropolis-Hastings (MH) MCMC algorithm to define a Markov Chain (MC) that samples from the posterior distributions of v and β . With the MH algorithm, we define the MC as a random walk through the parameter space of v and β . To generate m-th sample pair (v_m,β_m) of the posterior, we sample a candidate (v^*,β^*) using the following uncorrelated bivariate normal distribution

$$(\boldsymbol{v}^*, \boldsymbol{\beta}^*) \sim N\left(\mu_{(RW)}, \sigma_{(RW)}\right) \tag{8}$$

where $\mu_{(RW)}$ is the mean vector of the random walk, and it is equal to the last posterior sample (v_{m-1},β_{m-1}) . $\sigma_{(RW)}$ is the covariance matrix, equal to the diagonal matrix $diag(\sigma_{v\ (RW)},\sigma_{\beta\ (RW)})$. $\sigma_{v\ (RW)}$ and $\sigma_{\beta\ (RW)}$ are calibrated values for an effective exploration of the high-probability regions, i.e., good mixing. For this symmetrical random walk, the sample candidate (v^*,β^*) is accepted with probability $\min(1,A)$, where

$$A = \frac{p(x|v^*, \beta^*)p(v^*, \beta^*)}{p(x|v_{m-1}, \beta_{m-1})p(v_{m-1}, \beta_{m-1})}$$
(9)

According to the MH properties, the MC has a stationary distribution, i.e., the resulting distribution when the number of samples is sufficiently large, equal to the posterior distribution of v and β in Eq. (2).

This algorithm was implemented to assess the posterior of the fragility function parameters for both rooftop and ground-mounted panels. We ensured a good mixing by calibrating $\sigma_{v\ (MCMC)}$ and $\sigma_{\beta\ (RW)}$ such that the average acceptance rate is around 25% as recommended in the literature [54,55]. Using the MH MCMC analysis, we sampled 10, 000 realizations of v and β from the posterior distribution after a burn-in period containing 1000 realizations. We selected the burn-in period after verifying the MC stationarity (Supplementary Fig. 2).

4. Bayesian updates for fragility functions

4.1. Rooftop panels

We used the generated 10,000 samples to estimate the posterior distribution of the fragility function parameters. For v, the median varied from 85 m/s in the prior to 80 m/s in the posterior, its standard deviation from 51 to 5 m/s, and its logarithmic standard deviation from 0.5 to 0.07 (Fig. 5a). The similar prior and posterior medians show that the numerical analysis in Goodman [13] is consistent with the observations of wind in terms of the 50%-failure probability. The significant decrease (90%) in the standard deviation reveals the importance of the solar panel dataset in decreasing the initial epistemic uncertainties of v.

For β , the median varied from 0.13 in the prior to 0.32 in the posterior, its standard deviation from 0.08 to 0.11, and its logarithmic standard deviation from 0.5 to 0.30 (Fig. 5b). The posterior median of β is almost three times the prior value. Such an increase reveals the inconsistency of the numerical analysis in Goodman [13] with the empirical data in terms of the aleatory uncertainty measured by β . The numerical analysis implies that the transition range between winds with low and high failure probabilities is narrow. Conversely, previous empirical evidence [56,57] suggests that the β value of 0.13 is too small to characterize the uncertainty in wind hazards, implying a wider transition range between winds with low and high failure probabilities. This observation demonstrates the importance of empirical data to calibrate numerical analysis.

We found a lack of correlation between v and β in the posterior as the Pearson's coefficient between their posterior samples was only $3x10^{-4}$. This result suggests independence between v and β , as assumed in the prior.

The Bayesian update from the parameters' prior distribution to the posterior distribution brings important implications for the fragility

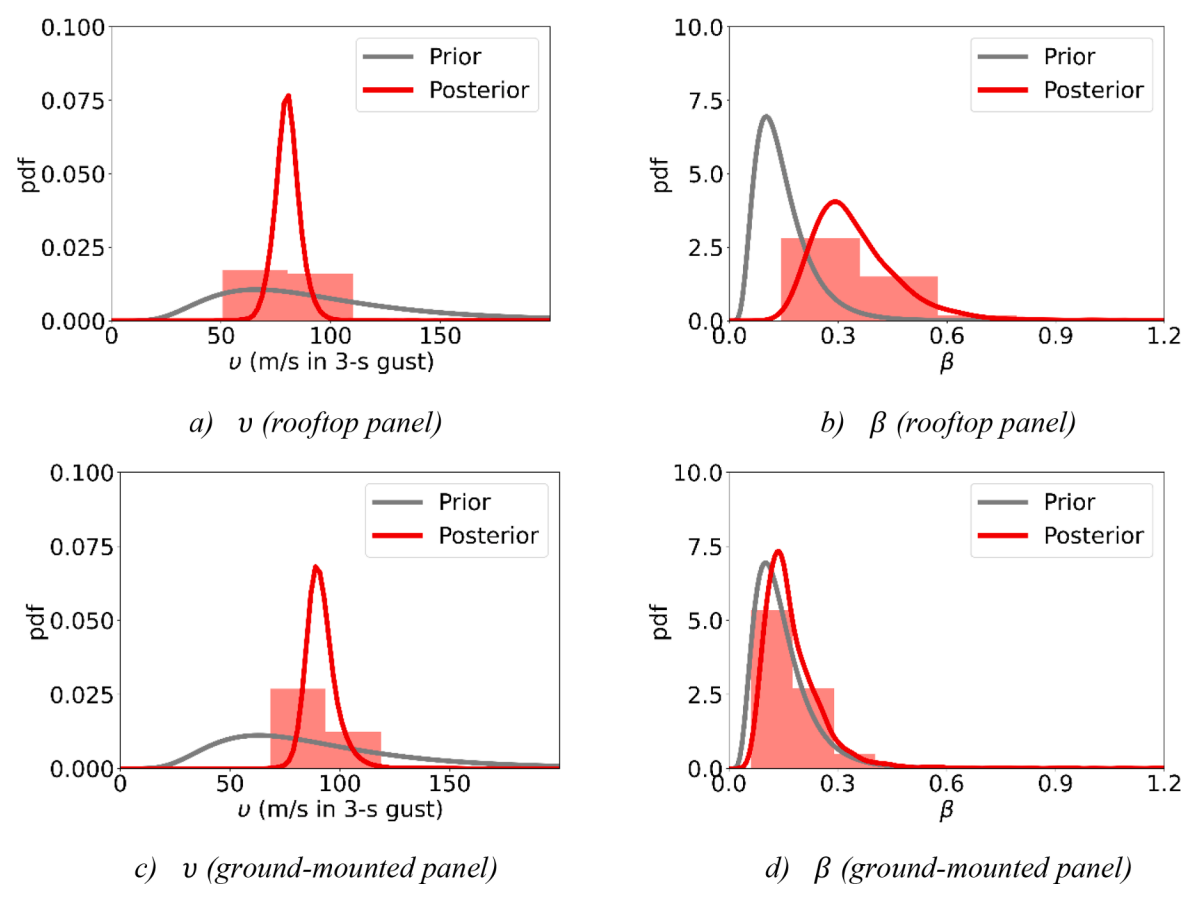


Fig. 5. The prior and posterior distribution of v and β for rooftop solar panels. Samples from the posterior distribution were used to depict the histogram, and Gaussian kernel was used to develop each empirical pdf.

function of rooftop solar panels. The mean fragility function, describing the probability of panel failure, for the posterior distribution can be found as

$$E[q(w)] = \int_{0}^{\infty} \int_{0}^{\infty} q(w; v, \beta) p(v, \beta | x) dv d\beta$$
 (10)

Eq. (10) uses the posterior $p(v,\beta|x)$ as the distribution of v and β to find the posterior of E[q(w)]. Replacing $p(v,\beta|x)$ by the prior $p(v,\beta)$ will result in the prior E[q(w)].

We solved Eq. (10) by averaging all q values for the suite of 10,000

fragility functions, obtained by evaluating the 10,000 samples of v and β (Fig. 6a). With this procedure, we incorporate and propagate the uncertainty in v and β to the fragility function. The deterministic prior distribution in Goodman [13] was used to set up the prior medians' hyperparameters. However, the resulting mean fragility function (E[q(w)]) from the Bayesian prior is different than its frequentist counterpart due to its parameters' uncertain nature. The difference is negligible for the wind with a 50%-failure probability (\sim 85 m/s for both). Yet, it is significant for the wind with a 10 and 90%-failure probability (71 versus 43 and 100 versus 167 m/s). The wider wind range in the transition from a 10% to a 90%-failure probability in the Bayesian

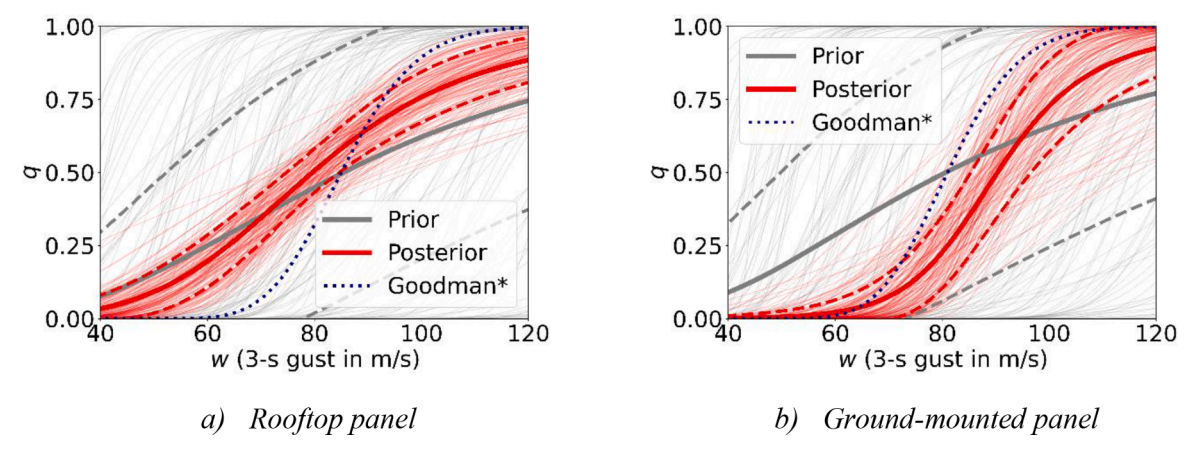


Fig. 6. Fragility functions for random samples v and β according to their prior and posterior distributions. The solid thicker lines indicate the expectation of the failure probability over the parameters' distribution, and the dashed lines indicate the mean plus and minus a standard deviation. Goodman* is the deterministic fragility function adapted from Goodman [13].

assessment results from the uncertainty propagation from v and β (Fig. 5a and b's gray curves) to the fragility function.

The posterior distribution changes the wind for 50%-failure probability only slightly (-5%), from 86 m/s in the prior to 80 m/s in the posterior. The wind range that transitions from a 10% to a 90%-failure probability, 52 and 123 m/s, respectively, has a width that is 56% smaller than the prior. This reduction results from the lower uncertainty in v, whose standard deviation decreases from 51 in the prior to 5 m/s in the posterior (Fig. 5a). Moreover, the posterior fragility function shows a significantly narrower confidence interval than the prior fragility function. These results demonstrate the importance of the Bayesian approach to capture and reduce large initial uncertainties through empirical data, not only in the fragility function parameters (v and β), but also in the mean fragility function itself.

4.2. Ground-mounted panels

The distribution of v shows that the median varies from 81 m/s in the prior to 90 m/s in the posterior, its standard deviation from 50 m/s to 6 m/s, and its logarithmic standard deviation from 0.5 to 0.07 (Fig. 5c). The posterior shows a significant reduction in the uncertainty in v, with a standard deviation 87% lower than that of the prior. Such a reduction is very close to the one found in rooftop solar panels, even though the number of data points is one-third of the latter.

For β , the median varies from 0.13 in the prior to 0.15 in the posterior, its standard deviation remains in 0.07, and its logarithmic standard deviation from 0.5 to 0.39 (Fig. 5d). As a result, the posterior distribution exhibits a slight shift to the right. The little variations in β 's standard deviation and logarithmic standard deviation suggest that the number of data points is insufficient to substantially reduce uncertainty.

Following the same procedure for the rooftop panels, we estimated the mean fragility function (E[q(w)]) for ground-mounted solar panels (Fig. 6b). Unlike the posterior fragility function for rooftop panels, the posterior fragility function for ground-mounted panels has a higher wind value (+10%) for a 50%-failure probability than its prior, 90 versus 81 m/s. This increase suggests that the panel installations for ground-mounted solar panels were structurally sounder than for rooftop panels, whose wind for 50%-failure probability in the posterior was 5% less than in the prior. This better structural performance may result from more code enforcement, better member and connection installation (e. g., avoiding loose bolts), or proper inspections [32,33]. These panels are part of large installations with massive investments from utility companies, which, unlike residential homes that install rooftop panels, often have a budget for appropriate quality and control.

We found that the wind range that transitions from a 10 to 90% failure probability in the posterior, 73 and 116 m/s, is reduced in 64% from the prior, 41 and 160 m/s. This narrower range is driven mainly by the lower standard deviation in v (Fig. 5c). This reduction in the transition range is larger than that in the case of the rooftop panels (Fig. 6) because, unlike the rooftop panels, the ground-mounted panels' posterior of β did not have a larger standard deviation than the prior. Furthermore, the posterior fragility function shows a much narrower confidence interval than the prior fragility function. However, the confidence interval is slightly wider than in rooftop panels because the ground-mounted panel dataset is only a third of the rooftop panel dataset.

5. Panel's annual failure rate

To illustrate their application, we use our fragility functions to assess solar panel risk for hurricane winds for Miami-Dade, Florida, as a case study. Miami-Dade is exposed to similar wind hazards in Puerto Rico. For example, the risk category II design wind (700-year return period) in San Juan, Puerto Rico, is 71 m/s (159 mph), whereas the design wind in Miami-Dade is 73 m/s (164 mph). Different standards for solar panel installation and code enforcement might be in place in Miami-Dade,

especially for rooftop panels, which performed worse than ground-mounted panels. However, more data collection efforts will be needed to confirm whether panels in mainland United States have fundamentally different structural behavior than those in the Caribbean. Due to the lack of these datasets, here we use our fragility functions from the Caribbean to study solar panels' reliability and resilience performance in Miami-Dade; analysis for other regions can be similarly performed.

A study site in the mainland United States is chosen to leverage a synthetic hurricane database with 5018 landfalling storms in the United States generated from a statistical-deterministic tropical cyclone (TC) model [31]. These synthetic hurricanes account for current climate conditions (from 1980 to 2005) according to the National Center for Environmental Prediction (NCEP) reanalysis. The 5018 synthetic storms correspond to ~1485 years of storm simulation. The model that generates these storms consists of three stages: a genesis model; a beta-advection TC motion model; and a dynamical TC model that captures how environmental factors influence TC development [58]. The model solves the synthetic storms' tracks, maximum sustained winds, and radii of maximum winds, and we use its results at 2 h intervals. We estimated the wind fields by combining the storm's axisymmetric winds circulating counterclockwise [37] and background winds [38], as in the wind analysis for the historical storms. The synthetic hurricanes were evaluated with observations by Marsooli et al. [31].

We determine the annual rate of panel failure λ_f by combining the wind simulations with the Bayesian fragility functions. The rate defines the average number of events leading to panel failures in a given year assuming a Poisson process. In a frequentist analysis, the fragility function parameters v and β are fixed. Thus, $\lambda_f(v,\beta)$ can be estimated as

$$\lambda_f(v,\beta) = \int\limits_0^\infty q(w;v,\beta)d\lambda_w \tag{11}$$

where λ_w is the annual exceedance probability of wind speed. It is the average number of events that result in winds exceeding a threshold w in a given year under a Poisson process of storm arrivals, and it can be estimated from the synthetic storms. In our Bayesian framework, v and β are random variables. Thus, λ_f is also a random variable. Accordingly, its probability density function $p_{\lambda_f}(\lambda)$ can be found as

$$\mathbf{p}_{\lambda_f}(\lambda) = \int\limits_0^\infty \int\limits_0^\infty p(v, \beta | x) \delta\left(\lambda - \int\limits_0^\infty q(w; v, \beta) d\lambda_w\right) dv d\beta \tag{12}$$

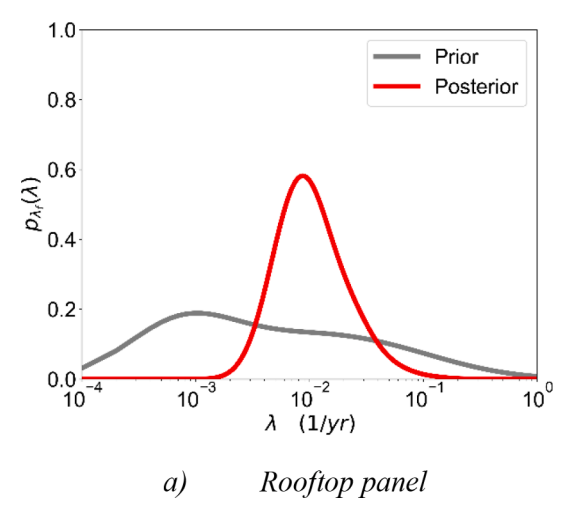
where $\delta()$ is the Dirac delta function on $\lambda - \int\limits_0^\infty q(w;v,\beta)d\lambda_{\rm w}$. Eq. (12) uses

the posterior $p(v,\beta|x)$ as the distribution of v and β to find the posterior of $\mathrm{p}_{\lambda_f}(\lambda)$. Replacing $p(v,\beta|x)$ by the prior $p(v,\beta)$ will result in the prior $\mathrm{p}_{\lambda_f}(\lambda)$. The expected value of λ_f , $\mathrm{E}[\lambda_f]$, can be found as:

$$E[\lambda_f] = \int_0^\infty \int_0^\infty \left[\int_0^\infty q(w; v, \beta) d\lambda_w \right] p(v, \beta | x) dv d\beta$$
 (13)

Explicitly evaluating $E[\lambda_f]$ and particularly $p_{\lambda_f}(\lambda)$ is computationally challenging by traditional numerical integration. Thus, we used Monte Carlo analysis due to its simplicity to find such estimates. Using the 10,000 Monte Carlo samples of prior and posterior fragility functions, we estimated the prior and posterior of λ_f (Fig. 7).

Our results indicate a marked decrease in uncertainty for λ_f in the posterior. The posterior standard deviation and logarithmic standard deviation for rooftop panels are $1.2\times 10^{-2}/\mathrm{yr}$ and 6.3×10^{-1} , whereas the priors' ones are $5.1\times 10^{-2}/\mathrm{yr}$ and 1.82. The posterior standard deviation and logarithmic standard deviation for ground-mounted panels are $1.7\times 10^{-3}/\mathrm{yr}$ and 5.5×10^{-1} , whereas the priors' ones are $5.7\times 10^{-2}/\mathrm{yr}$ and 1.87. This uncertainty decrease in the annual failure



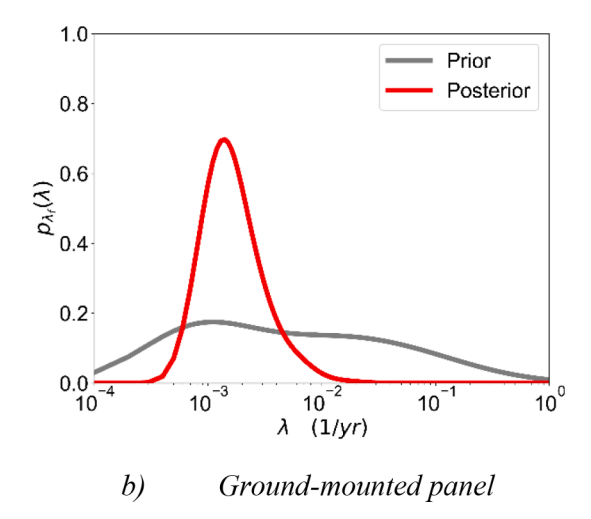


Fig. 7. Probability density function $p_{i_g}(\lambda)$ of the annual probability of failure rate of solar panels. Samples from the Monte Carlo simulations were used to fit empirical pdfs with a Gaussian kernel.

rate is consistent with the observed posterior fragility function uncertainty reductions for rooftop and ground-mounted panels (Fig. 6).

For rooftop panels, the posterior $E[\lambda_f]$ is $1.3 \times 10^{-2}/yr$, i.e., return period of 75 years. Under the assumption of a Poisson process, this rate results in a 48% probability of failure in 50 years. This rate is equivalent to a 33% failure probability in 30 years, often considered the usable panel service time. The reliability index, defined as the inverse of the cumulative standard normal distribution function on the survival probability, i.e., one minus the failure probability, in 50 years, is 0.04. This reliability is significantly lower than the current standards in the ASCE7-16. Using reliability curves from a recent study on wind risks [59], we estimated that a structure designed for winds with a 700-year return period (risk category II) should have a reliability index of 2.3 in 50 years, i.e., failure rate of $2.3 \times 10^{-4}/yr$. Thus, our findings show that the structural reliability of rooftop solar panels in our dataset was significantly below current code standards if similar panels are adopted in Miami-Dade. These results are consistent with the observed structural deficiencies in the installation and design of panels with failures in the dataset, e.g., insufficient connection strength, lack of vibration-resistant connections [32]. Thus, significant gains in reliability could be achieved by increasing quality and control during design and installation.

For ground-mounted panels, the posterior $E[\lambda_f]$ is 2.0×10^{-3} /yr, i.e., return period of 504 years. This rate is equivalent to a 9 and a 6% probability of failure in 50 and 30 years, respectively. The reliability index for 50 years is 1.3. According to the ASCE7-16, the reliability index for a structure designed for winds with a 300-year return period (risk category I) is 1.9, i.e., failure rate of 6.1×10^{-4} /yr [59]. Thus, our results indicate that ground-mounted panels also have lower reliability than required by the current code standards. These results are also consistent with previously reported structural deficiencies in ground-mounted panels in the Caribbean, e.g., undersized racks, and undersized or under-torqued bolts [33]. Nevertheless, the contrast between rooftop and ground-mounted panel performance indicates that the latter had a significantly higher structural reliability than the former.

6. Stronger solar panels for generation resilience

6.1. Assessing structural reliability and generation in stronger panels

We assessed panels' strength increases by factors of 1.25, 1.50, 1.75, and 2.0. This wide range of strength increases accounts for addressing various panel installations and design deficiencies reported in the Caribbean. Existing studies already point to cost-effective solutions to correct these deficiencies, e.g., torque checks on bolts, well-designed

clips [32,33].

This range also covers increases in strength for critical infrastructure. Hospitals and fire stations require that their buildings' structural and non-structural components have higher strength for continuous operations in a disaster emergency response. Accordingly, solar panels serving these facilities must be designed with a risk category IV, higher than for panels on residential (risk category II) or utility-scale (risk category I) installations. For example, the wind design in Miami-Dade is 69 m/s (154 mph) for a risk category I and 81 m/s (182 mph) for a risk category IV. The difference represents a strength factor of 1.40 as the design force is proportional to the square of the design wind.

Wind velocity pressures are a function of the square root of wind speeds [7]. Thus, we multiplied the posterior samples of (capacities of) wind speeds v by 1.12, 1.22, 1.32, 1.41 to represent the strength increase factors of 1.25, 1.50, 1.75, and 2.0. We let samples of ρ remain the same to limit the increase in uncertainty, i.e., the transition from low-failure-probability to high-failure-probability winds. The resulting fragility functions are shifted to the right of the posterior functions in Fig. 6, reducing the likelihood of panel failure (Fig. 8). For example, the mean failure probability q when rooftop panels undergo gusts of 60 m/s decreases from 0.19 to 0.12, 0.08, 0.05, and 0.04 for the strength factors of 1.25, 1.50, 1.75, and 2.0, respectively. Similarly, the mean q when ground-mounted panels undergo gusts of 80 m/s decreases from 0.23 to 0.09, 0.04, 0.02, and 0.01.

Using Monte Carlo sampling, we estimated $p_{\hat{i}_f}(\lambda)$ for the different increases in strength (Fig. 9). Expectedly, increases in strength shift $p_{\hat{i}_f}(\lambda)$ to the left as they reduce the resulting annual rate of failure. We also found $E[\lambda_f]$ and assessed the corresponding panels' structural reliability (Table 2). The increases in strength are effective at decreasing $E[\lambda_f]$. The strength factor of two reduces $E[\lambda_f]$ by a factor of 3.9 and 2.5 for rooftop and ground-mounted panels, respectively. A more modest strength factor of 1.25 also effectively decreases panel failure risk, reducing $E[\lambda_f]$ by ~50% and ~70% for rooftop and ground-mounted panels, respectively. Nevertheless, our results indicate that the reliability indexes for these stronger panels are still below the ASCE7-10 targets even for a risk category I, i.e., 1.9.

These results highlight large structural vulnerabilities in solar panels since they do not reach code-level reliability even if their strength is increased twice. These results suggest that existing lack of structural design and limited inspections in the panel installations were significant [32,33]. High vulnerability to hurricane winds has been noted previously in buildings. For example, a previous study in Southern Florida determined that roof-to-wall connections with 3-8d toenails in wooden residential buildings have an annual failure rate between 0.005 and

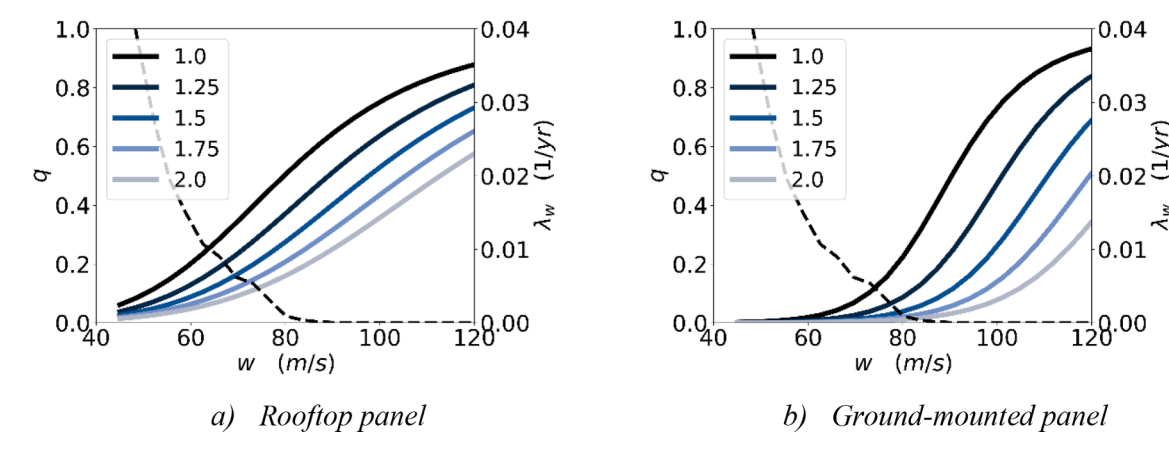


Fig. 8. Mean fragility functions for panels with increases in strength. The factors that multiply each *v* sample are equal to the square root of the strength factors in the labels. The dashed curves indicate the wind annual exceedance rates. The x-axis represents 3 s gusts.

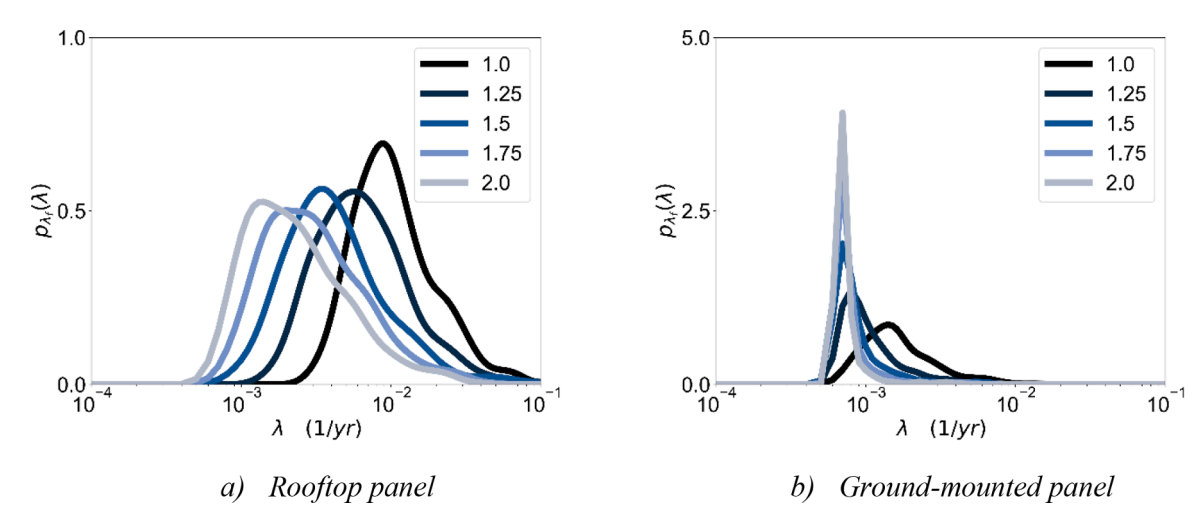


Fig. 9. Probability density function of the annual failure rate of solar panels for different increases in panel strength. The labels indicate the strength factor increase.

Table 2Annual probability of panel failure and reliability indexes (for 50 years) for different increases in strength.

Strength Factor	Rooftop pane	Rooftop panel		Ground-mounted panels	
	$E[\lambda_f] (1/yr)$	Reliability index	$E[\lambda_f] (1/yr)$	Reliability index	
1.0	0.0132	0.04	0.0020	1.30	
1.25	0.0089	0.36	0.0012	1.58	
1.50	0.0061	0.63	0.0010	1.66	
1.75	0.0043	0.87	0.0009	1.73	
2.0	0.0034	1.01	0.0008	1.77	

0.024~[60]. These rates are comparable to the rooftop panels in our case study and below the performance of ground-mounted panels (Table 2). Furthermore, roof panels with 6d nails @ 6/12 in. on these buildings showed even poorer performance, with higher annual failure rates of 0.077-0.137.

6.2. Will stronger solar panels increase generation resilience?

As demonstrated previously, increasing panel strength will increase its reliability. However, other critical factors also play a significant role in solar generation resilience, i.e., the ability to generate sufficient electricity during storms. First, solar generation can decrease even if panels remain structurally sound and functional during a hurricane.

Ceferino et al. [61] demonstrated that hurricane clouds can reduce irradiance and generation significantly through light absorption and reflection. For example, a category-4 hurricane can decrease the generation by more than 70%, even if the panels remain undamaged. Cloud-driven generation losses can last for days, although they will bounce back to normal conditions in an undamaged panel as the hurricane leaves.

Failure of supporting infrastructure can also decrease generation resilience even if panels withstand extreme wind loads. Increasing the strength of rooftop panels on vulnerable roofs will not increase the global reliability of the residential energy system. Global reliability must consider that panels can fail in a cascading failure triggered by roof uplift, damaging the panel or its connections. The weakest link will control the reliability of this in-series system. As mentioned previously, roof-to-wall connections with 3-8d toe nails or roof panels with 6d nails @ 6/12" exhibited similar or poorer performance than vulnerable rooftop panels [60]. Strengthening panels on these roofs will substantially increase their local reliability (Table 2), but it will increase global reliability only negligibly. Conversely, roofs with H2.5 hurricane clips in roof-to-wall connections and 8d nails @ 6/12' in roof panels will make roofs an appropriate supporting system through higher reliability [60]. Thus, our results advocate for stronger panels but under a holistic assessment of global reliability.

Structurally sound rooftop panels have the intrinsic advantage of delivering power even if the primary grid is down. When inverters are within buildings, occupants can use their locally generated energy during an outage (Cook et al., 2020) to sustain essential functions, e.g., food refrigeration. Access to energy is also pivotal to sustaining emergency response operations for critical infrastructure such as hospitals or fire stations. Communities can further utilize locally generated energy through energy sharing and microgrids to increase households' access to power after a disaster, even for those who did not install panels [62,63]. Nevertheless, solar panels will not replace the need for backup generation units for resilience, especially for critical facilities, and fully charged behind-the-meter batteries must complement them for power access during an emergency response.

Stronger panels will also increase power security at the utility level by avoiding massive structural failures at the generation sites, as in Fig. 1b. As noted previously, solar panels are directly exposed to wind. Poor structural performance in utility companies' solar installations could result in significant generation losses and outages that can affect the disaster emergency response and recovery activities. Recently, Hurricane Ida caused damage to the power system that resulted in $\sim\!\!1\,\mathrm{M}$ outages in Louisiana, reducing electricity access by more than 60% in more than ten parishes (counties), critically affecting the functionality of the water system and delaying recovery [64,65]. While solar generation losses could be potentially offset by other generating sources during an emergency response, adopting vulnerable panels in our grid will be a missed opportunity to make our power systems resilient.

7. Conclusions

This paper presented the first data-driven fragility curves for solar panels under hurricane wind loads. The article estimated the fragility curves using data on the structural performance of 46 rooftop panels in residential buildings and 14 large ground-mounted solar panel arrays in utility generation sites. Solar panel failure data was collected after Hurricanes Maria and Irma in 2017 and Hurricane Dorian in 2019 in the Caribbean. Further, this paper assessed solar generation resilience and its improvements with stronger panels.

We used a Bayesian approach to supplement the panel dataset with an existing numerical assessment of panel failure. Using a Markov Chain Monte Carlo algorithm, we estimated the posterior distributions of fragility parameters for the rooftop and ground-mounted panels separately. Our results show significant reductions in epistemic uncertainty for v (wind for a 50%-failure probability) in rooftop and ground-mounted panels with 90 and 87% decreases in the standard deviation. Using Monte Carlo, we then propagated the uncertainty in the parameters to the fragility functions, showing significantly narrower confidence intervals. This result highlighted the importance of characterizing fragility functions with ground-truth data.

We combined our fragility functions with a hurricane hazard assessment in Miami-Dade, Florida, using Monte Carlo simulations. Miami-Dade has similar hurricane hazards to Puerto Rico, where most damage data was collected. Our estimates of the annual rate of panel structural failure indicated that the panels are below the current structural reliability standards specified in ASCE7-16. These performance deficiencies were particularly striking for rooftop panels (estimated failure rate of $1.3 \times 10^{-2}/yr$ versus $2.3 \times 10^{-4}/yr$ in the code), whose documented installation issues and frequent lack of structural design made them particularly vulnerable to high winds.

Finally, we analyzed the implications of building stronger solar panels by up to a factor of two due to improvements in the panels' installations, structural design, or higher structural requirements. We show that increasing panel strength effectively reduces the annual failure rate. However, even the factor of two is still insufficient to meet annual failure rates in the ASCE7-10 (reliability index of 1.9 for the lowest risk category) for rooftop and ground-mounted panels (reliability indexes of 1.01 and 1.77).

CRediT authorship contribution statement

Luis Ceferino: Conceptualization, Methodology, Data curation, Formal analysis, Writing – original draft. **Ning Lin:** Conceptualization, Methodology, Formal analysis, Writing – review & editing. **Dazhi Xi:** Formal analysis, Writing – review & editing.

Declaration of Competing Interest

The authors declare that they have no conflict of interest.

Data availability

The data is provided in the Supplementary Information.

Acknowledgments

We thank Sanya Detweiler from the Clinton Foundation, Chris Needham and Solar Frank Oudheusden from FCX Solar, and Christopher Burgess from the Rocky Mountain Institute for sharing their reports, photos, and relevant documentation on solar panels' structural performance after Hurricanes Maria and Irma in 2017 and Dorian in 2019. We also acknowledge the financial support by the Andlinger Center for Energy and the Environment at Princeton University through the Distinguished Postdoctoral Fellowship. Additionally, this research was also supported by the NSF Grant 1652448. The authors are grateful for their generous support.

Supplementary materials

Supplementary material associated with this article can be found, in the online version, at doi:10.1016/j.ress.2022.108896.

References

- [1] Chowdhury MS, Rahman KS, Chowdhury T, Nuthammachot N, Techato K, Akhtaruzzaman M, Tiong SK, Sopian K, Amin N. An overview of solar photovoltaic panels' end-of-life material recycling. Energy Strategy Rev 2020;27:100431. https://doi.org/10.1016/j.esr.2019.100431.
- [2] Lan TT, Jirakiattikul S, Chowdhury MS, Ali D, Niem LD, Techato K. The effect of retail electricity price levels on the FI values of smart-grid rooftop solar power systems: a case study in the central highlands of vietnam. Sustainability 2020;12 (21):9209. https://doi.org/10.3390/su12219209.
- [3] Solaun K, Cerdá E. Climate change impacts on renewable energy generation. A review of quantitative projections. Renew Sustain Energy Rev 2019;116(109415). https://doi.org/10.1016/j.rser.2019.109415.
- [4] The International Renewable Energy Agency. Global energy transformation: a rodmap to 2050. Global energy transformation. the International Renewable Energy Agency; 2018.
- [5] Perea A, Smith C, Davis M, Mond A, Gallagher B, Rumery S, et al. U. S. Solar Market Insight Executive Summary. Wood Mackenzie & Solar Energy Industries Association 2019.
- [6] U.S. Energy Information Administration. (2021). Electricity explained: Electricity generation, capacity, and sales in the United States. https://www.eia.gov/energyexplained/electricity/electricity-in-the-us-generation-capacity-and-sales.php. Accessed: 10/13/2022.
- [7] American Society of Civil Engineers. Minimum design loads and associated criteria for buildings and other structures. Minimum design loads and associated criteria for buildings and other structures. American Society of Civil Engineers; 2017. https://doi.org/10.1061/9780784414248.
- [8] Cain JH, Banks D, Petersen CP. Wind loads on utility scale solar PV power plants. In: Proceedings of the SEAOC convention proceedings; 2015. p. 1–8. http://www.cppwind.com/wp-content/uploads/2014/01/Wind-Loads-on-Utility-Scale-Solar-PV-Power-Plants DBanks 2015.pdf.
- [9] Arora, P., & Ceferino, L. (2022). Probabilistic and machine learning methods for uncertainty quantification in power outage prediction due to extreme events Preprint, October, 1–29 doi:10.5194/egusphere-2022-975.
- [10] Bennett JA, Trevisan CN, Decarolis JF, Ortiz-garcía C, Pérez-lugo M, Etienne BT, Clarens AF. Extending energy system modelling to include extreme weather risks and application to hurricane events in Puerto Rico. Nat Energy 2021;6. https://doi. org/10.1038/s41560-020-00758-6. March.
- [11] Winkler J, Dueñas-Osorio L, Stein R, Subramanian D. Performance assessment of topologically diverse power systems subjected to hurricane events. Reliab Eng Syst Saf 2010;95(4):323–36. https://doi.org/10.1016/j.ress.2009.11.002.

- [12] Zhai C, Chen TYjeh, White AG, Guikema SD. Power outage prediction for natural hazards using synthetic power distribution systems. Reliab Eng Syst Saf 2021;208. https://doi.org/10.1016/j.ress.2020.107348. November 2020.
- [13] Goodman, J. N. (2015). Performance Measures for Residential PV Structural Response to Wind Effects. Ph.D. Thesis. Civil and Environmental Engineering Department, Georgia Institute of Technology.

L. Ceferino et al.

- [14] Watson, E. B. (2018). Modeling Electrical Grid Resilience under Hurricane Wind Conditions with Increased Solar Photovoltaic and Wind Turbine Power Generation. Ph.D. Thesis. The School of Engineering and Applied Sciene, The George Washington University. https://doi.org/10.1542/peds.2006-2099.
- [15] Kwasinski A. Effects of hurricane maria on renewable energy systems in Puerto Rico. In: Proceedings of the 7th international IEEE conference on renewable energy research and applications, ICRERA 2018. 5; 2018. p. 383–90. https://doi.org/ 10.1109/ICRERA.2018.8566922.
- [16] Singhal A, Kiremidjian AS. Bayesian updating of fragilities with application to RC frames. J Struct Eng 1998;124(8):922–9. https://doi.org/10.1061/(ASCE)0733-9445(1998)124-8(922)
- [17] Ceferino L, Galvez P, Ampuero JP, Kiremidjian A, Deierlein G, Villegas-Lanza JC. Bayesian parameter estimation for space and time interacting earthquake rupture model using historical and physics-based simulated earthquake catalogs. Bull Seismol Soc Am 2021;111(6):3356–73. https://doi.org/10.1785/0120210013.
- [18] Choe DE, Gardoni P, Rosowsky D. Closed-form fragility estimates, parameter sensitivity, and bayesian updating for RC columns. J Eng Mech 2007;133(7): 833–43. https://doi.org/10.1061/(asce)0733-9399(2007)133:7(833).
- [19] der Kiureghian A, Melchers RE, Stewart MG. A Bayesian framework for fragility assessment. editor. In: Proceedings of the 8th international conference on applications of statistics and probability; 1999. p. 219–26.
- [20] Gardoni P, der Kiureghian A, Mosalam KM. Probabilistic capacity models and fragility estimates for reinforced concrete columns based on experimental observations. J Eng Mech 2002;128(10):1024–38. https://doi.org/10.1061/(asce) 0733-9399(2002)128:10(1024).
- [21] Gardoni P, Mosalam KM, der Kiureghian A. Probabilistic seismic demand models and fragility estimates for RC bridges. J Earthq Eng 2003;7:79–106. https://doi. org/10.1080/13632460309350474.
- [22] Huang Q, Gardoni P, Hurlebaus S. Probabilistic seismic demand models and fragility estimates for reinforced concrete highway bridges with one single-column bent. J Eng Mech 2010;136(11):1340–53. https://doi.org/10.1061/(ASCE) FM.1943-7889.0000186.
- [23] Koutsourelakis PS. Assessing structural vulnerability against earthquakes using multi-dimensional fragility surfaces: a Bayesian framework. Probab Eng Mech 2010;25(1):49–60. https://doi.org/10.1016/j.probengmech.2009.05.005.
- [24] Li J, Spencer BF, Elnashai AS. Bayesian updating of fragility functions using hybrid simulation. J Struct Eng 2013;139(7):1160–71. https://doi.org/10.1061/(asce) st.1943-541x.0000685.
- [25] Noh HY, Kiremidjian A, Ceferino L, So E. Bayesian updating of earthquake vulnerability functions with application to mortality rates. Earthq Spectra 2017;33 (3):1173–89. https://doi.org/10.1193/081216EOS133M.
- [26] Zhong J, Gardoni P, Rosowsky D, Haukaas T. Probabilistic seismic demand models and fragility estimates for reinforced concrete bridges with two-column bents. J Eng Mech 2008;134(6):495–504. https://doi.org/10.1061/(ASCE)0733-9399 (2008)134-6(495).
- [27] Jeon JS, Mangalathu S, Song J, Desroches R. Parameterized seismic fragility curves for curved multi-frame concrete box-girder bridges using bayesian parameter estimation. J Earthq Eng 2019;23(6):954–79.
- [28] Lei X, Sun L, Xia Y. Seismic fragility assessment and maintenance management on regional bridges using bayesian multi-parameter estimation. Bull Earthq Eng 2021; 19(15):6693–717.
- [29] Qin H, Stewart MG. Construction defects and wind fragility assessment for metal roof failure: A Bayesian approach. Reliab Eng Syst Saf 2020;197:106777. https://doi.org/10.1016/j.ress.2019.106777.
- [30] Zhang Y, Tien I. Conjugate Bayesian updating of analytical fragility functions using dynamic analysis with application to corroded bridges. Comput Struct 2022;270: 106832. https://doi.org/10.1016/j.compstruc.2022.106832.
- [31] Marsooli R, Lin N, Emanuel K, Feng K. Climate change exacerbates hurricane flood hazards along US Atlantic and Gulf coasts in spatially varying patterns. Nat Commun 2019;10(1):1–9. https://doi.org/10.1038/s41467-019-11755-z.
- [32] Burgess C, Detweiler S, Needham C, Oudheusden F. Solar Under Storm Part II: Select Best Practices for Resilient Roof-Mount PV Systems with Hurricane Exposure. Clinton Foundation, FCX Solar, and Rocky Mountain Institute; 2020 https://rmi.org/solar-under-storm-part-ii-designing-hurricane-resilient-pv-systems/
- [33] Burgess C, Goodman J. Solar Under Storm. Select Best Practices for Resilient Ground-Mount PV Systems with Hurricane Exposure. Rocky Mountain Institute; 2018.https://rmi.org/wp-content/uploads/2018/06/Islands_SolarUnderStorm Report_digitalJune122018.pdf.
- [34] National Oceanographic and Atmospheric Administration. (2021). Hurricane Maria Imagery. https://storms.ngs.noaa.gov/storms/maria/index.html#16/. Accessed: 12/05/2021.
- [35] Institute for Energy Research. (2018). Much of Puerto Rico's Wind and Solar Power Is Not Yet Operational. https://www.instituteforenergyresearch.org/the-grid/much-of-puerto-ricos-wind-and-solar-power-is-not-yet-operational/. Two renewable facilities on Puerto,Rico's fastest growing renewable resource. Accessed: 10/13/2022.
- [36] Landsea CW, Franklin JL. Atlantic hurricane database uncertainty and presentation of a new database format. Mon Weather Rev 2013;141(10):3576–92. https://doi. org/10.1175/MWR-D-12-00254.1.

- [37] Chavas DR, Lin N, Emanuel K. A model for the complete radial structure of the tropical cyclone wind field. Part I: comparison with observed structure. J Atmos Sci 2015;72(9):3647–62. https://doi.org/10.1175/JAS-D-15-0014.1.
- [38] Lin N, Emanuel K, Oppenheimer M, Vanmarcke E. Physically based assessment of hurricane surge threat under climate change. Nat Clim Chang 2012;2(6):462–7. https://doi.org/10.1038/nclimate1389.
- [39] NOAA National Centers for Environmental Information. (2001). Global Surface Hourly (Wind). NOAA National Centers for Environmental Information. https:// www.ncei.noaa.gov/. Accessed: 12/12/2021.
- [40] Vickery P, Skerlj P. Hurricane gust factors revisited. J Struct Eng 2005;131(5): 825–32. https://doi.org/10.1061/(ASCE)0733-9445(2005)131.
- [41] Ellingwood BR, Rosowsky DV, Li Y, Kim JH. Fragility assessment of light-frame wood construction subjected to wind and earthquake hazards. J Struct Eng 2004; 130(12):1921–30. https://doi.org/10.1061/(ASCE)0733-9445(2004)130:12 (1921).
- [42] Shinozuka M, Feng MQ, Lee J, Naganuma T. Statistical analysis of fragility curves. J Eng Mech 2000;126(12):1224–31. https://doi.org/10.1061/(ASCE)0733-9399 (2000)126:12(1224).
- [43] Straub D, der Kiureghian A. Improved seismic fragility modeling from empirical data. Struct Saf 2008;30(4):320–36. https://doi.org/10.1016/j. strusafe.2007.05.004.
- [44] Gokkaya BU, Baker JW, Deierlein GG. Quantifying the impacts of modeling uncertainties on the seismic drift demands and collapse risk of buildings with implications on seismic design checks. Earthq Eng Struct Dyn 2016;45(10): 1661–83. https://doi.org/10.1002/eqe.2740.
- [45] James MN. Residual stress influences on structural reliability. Eng Fail Anal 2011; 18(8):1909–20. https://doi.org/10.1016/j.engfailanal.2011.06.005.
- [46] Jiang Z, Hu W, Dong W, Gao Z, Ren Z. Structural reliability analysis of wind turbines: a review. Energies 2017;10(12):1–25. https://doi.org/10.3390/ en10122099.
- [47] Joung TH, Lee JH, Nho IS, Kim BJ, Han SH, Park SH, Lee CM, Lee PM, Sammut K, He F. A study on the design and manufacturing of a deep-sea unmanned underwater vehicle based on structural reliability analysis. Sh Offshore Struct 2009;4(1):19–29. https://doi.org/10.1080/17445300802315367.
- [48] Trbojevic VM. Another look at risk and structural reliability criteria. Struct Saf 2009;31(3):245–50. https://doi.org/10.1016/j.strusafe.2008.06.019.
- [49] Mohammadi Darestani Y, Shafieezadeh A. Multi-dimensional wind fragility functions for wood utility poles. Eng Struct 2019;183(November 2018):937–48. https://doi.org/10.1016/j.engstruct.2019.01.048.
- [50] Shafieezadeh A, Onyewuchi UP, Begovic MM, Desroches R. Age-dependent fragility models of utility wood poles in power distribution networks against extreme wind hazards. IEEE Trans Power Deliv 2014;29(1):131–9. https://doi.org/ 10.1109/TPWRD.2013.2281265.
- [51] Lee KH, Rosowsky DV. Fragility assessment for roof sheathing failure in high wind regions. Eng Struct 2005;27(6):857–68. https://doi.org/10.1016/j. engstruct.2004.12.017.
- [52] Quilligan A, O'Connor A, Pakrashi V. Fragility analysis of steel and concrete wind turbine towers. Eng Struct 2012;36:270–82. https://doi.org/10.1016/j. engstruct.2011.12.013.
- [53] Liu JS. Monte carlo strategies in scientific computing. New York: Springer; 2004. https://doi.org/10.1007/978-0-387-76371-2.
- [54] Chib S, Greenberg E. Understanding the metropolis-hastings algorithm. Am Stat 1995;49(4):327–35. http://www.jstor.org/stable/2684568.
- [55] Robert CP. The metropolis-hastings algorithm. Wiley StatsRef: statistics reference online. 2014. p. 1–15. https://doi.org/10.1002/9781118445112.stat07834.
- [56] Roueche DB, Lombardo FT, Prevatt DO. Empirical approach to evaluating the tornado fragility of residential structures. J Struct Eng 2017;143(9):04017123. https://doi.org/10.1061/(asce)st.1943-541x.0001854.
- [57] Roueche DB, Lombardo FT, Smith DJ, Krupar RJ. Fragility assessment of wind-induced residential building damage caused by hurricane harvey. 2017. Forensic Engineering 2018: Forging Forensic Frontiers. In: Proceedings of the 8th congress on forensic engineering; 2018. p. 1039–48. https://doi.org/10.1061/9780784482018.100. 1984.
- [58] Emanuel K, Sundararajan R, Williams J. Hurricanes and global warming: results from downscaling IPCC AR4 simulations. Bull Am Meteorol Soc 2008;89(3): 347–68. https://doi.org/10.1175/BAMS-89-3-347.
- [59] McAllister TP, Wang N, Ellingwood BR. Risk-informed mean recurrence intervals for updated wind maps in ASCE 7-16. J Struct Eng 2018;144(5):06018001. https:// doi.org/10.1061/(asce)st.1943-541x.0002011.
- [60] Li Y, Ellingwood BR. Hurricane damage to residential construction in the US: importance of uncertainty modeling in risk assessment. Eng Struct 2006;28(7): 1009–18. https://doi.org/10.1016/j.engstruct.2005.11.005.
- [61] Ceferino L, Lin N, Xi D. Stochastic modeling of solar irradiance during hurricanes. Stoch Environ Res Risk Assess 2022;36(9):2681–93.
- [62] Ceferino L, Liu C, Alisjahbana I, Patel S, Sun T, Kiremidjian A, Rajagopal R. Earthquake resilience of distributed energy resources. In: Proceedings of the 17th world conference on earthquake engineering; 2020.
- [63] Patel S, Ceferino L, Liu C, Kiremidjian A, Rajagopal R. The disaster resilience value of shared rooftop solar systems in residential communities. Earthq Spectra 2021;37 (4):2638–61. https://doi.org/10.1177/87552930211020020.
- [64] Hauser C. 31). Ida Evacuees Are Told to Stay Away From Louisiana Cities in Crisis. New York Times 2021, August. https://www.nytimes.com/live/2021/08/31/us/hurricane-ida-updates.
- [65] Prevatt D., Kameshwar S., Roueche D., Rittelmeyer B., Duarte T., Heo T., et al. StEER: Hurricane Ida Joint Preliminary Virtual Reconnaissance Report - Early Access Reconnaissance Report (PVRR-EARR) (Issue August). Structural Extreme

Event Reconnaissance (StEER) Network 2021. https://doi.org/10.17603/ds2-w6km-fe51.